DEVELOPMENT OF AN INKJET CARRIAGE MOTION CONTROLLER FOR DYNAMIC PRINT MODE CONTROL

A.V. Deshpande[a], M. Kamasak[c], K.L. Thoon[c]
G.T.-C. Chiu[b], C. Bouman[c], J. Allebach[c]

[a]*Real-Time Innovations, Sunnyvale, CA*

[b] *School of Mechanical Engineering,*
[c] *School of Electrical and Computer Engineering*
Purdue University, West Lafayette, Indiana

S. Fedigan, D. Schafer, C. Cole

Texas Instruments, Dallas, Texas

Abstract: Typical inkjet printers print with a variety of user-selectable print modes, where media, cartridge and image processing attributes are statically defined for each print mode. In this paper, we present the development of an inkjet carriage motion control system in which the carriage motion attributes can be dynamically changed depending on the image content. The resulting system enables the development of Dynamic Print Mode Control (DPMC). DPMC achieves optimal trade-off between print quality and print speed by selecting an appropriate printing attributes based on arbitrary segmentations of different image contents. The two-degree-of-freedom (TDOF) controller combines a disturbance observer with a filtered zero-phase error tracking controller (ZPETC) for high tracking performance under uncertain disturbances and model uncertainties. Experimental results show an excellent performance under fixed-point controller implementation.

Keywords: Printers, motion control, digital signal processors

1. INTRODUCTION

Typical inkjet printers print with a variety of user-selectable print modes that are compromises between quality and throughput. These print modes control the media advance, cartridge motion and image processing attributes, such as number of passes, print direction, print-head (cartridge) speed, print mask and halftoning techniques. Print quality of different image contents such as continuous tone image, graphics, line art and text is directly affected by the specific print mode chosen. Tables 1 and 2 show the measured values of some of these attributes for the black and color cartridge from a typical personal inkjet printer.

High quality print modes are characterized by slower carriage speeds often combined with uni-directional printing to reduce printing artifacts associated with bi-directional printing. This results in the high quality printing of continuous tone images at the expense of decreased throughput. Low quality print modes, while sacrificing the print quality increase the throughput with higher carriage speeds and bi-directional printing. Media advance for a given print mode is determined by the corresponding number of passes that governs the print masking and halftoning strategy. User selection of these print modes statically defines the motion parameters for the corresponding print mode. Printer manufacturers use a variety of techniques to improve this trade-off between throughput and print quality.

The carriage motion can be divided into two separate zones. In the *print zone*, the carriage needs to maintain a constant speed and the ink is fired at a constant interval. In the *non-print zone*, the carriage can accelerate or decelerate or travel at a higher speed to improve performance. Since no printing is done, motion control requirement is less strict. The maximum printhead speed is a function of the maximum firing rate of the inkjet cartridge, available motor torque and the length of the non-print zone. Increasing motor torque output or increasing the length of non-print zone are possible ways to improve print speed.

In one approach to increase effective print speed [1], the printer controller previews the printable data in each swath to determine the maximum acceleration period available from current carriage position and accelerates the carriage within this time period to print at the desired speed. In majority of cases, this will result in higher than normal print speed used to print the data. Since significant time is also spent in advancing the media, in another

invention [2], printer throughput is increased by overlapping carriage deceleration/acceleration turn around period with advancing the media.

Table 1: Measurements of print attributes for the color cartridge (Nozzle height is 192 nozzles, 64 nozzles each for cyan, magenta and yellow)

Printmode / Attributes	Draft Mode	Normal Mode	High Mode	Max. Mode
No. of passes/ No. of nozzles	1/64	2/32	4/16	8/8
Printing Direction	bi-dir	bi-dir	uni-dir	uni-dir
Cartridge speed (ips)	40	40	30	30

Table 2: Measurements of print attributes for the black cartridge (Nozzle height is 208 nozzles)

Printmode / Attributes	Draft Mode	Normal Mode	High Mode	Max. Mode
No. of passes/ No. of nozzles	1/208	2/104	4/52	8/26
Printing Direction	bi-dir	bi-dir	uni-dir	uni-dir
Cartridge speed (ips)	30	20	20	20

The cartridge transport mechanism may either be actuated by a stepper motor in open loop [3] or a DC motor in closed loop [1,2,4]. Instead of constant acceleration, the velocity is increased in successive acceleration steps to allow the velocity transients to subside before applying subsequent acceleration steps [3]. This is especially useful in open loop operation.

Another method to improve print speed is to reduce the percentage of non-print zones. One approach to reduce the non-print zone is to provide cartridge nozzle firing hardware, which is capable of printing while accelerating or decelerating [4, 5]. If ink is dispersed only when carriage velocity becomes constant, the length of non-print zone in the low quality modes may be longer than that in the higher quality modes due to higher carriage speed in low quality modes. To reduce this length, some printers [6] start printing in lower quality modes before carriage reaches the constant slew/printing speed. If acceleration ramp and deceleration ramp portion of the motion trajectory can be of different lengths [6], this asymmetrical acceleration ramp area can be effectively used with printing at less than full carriage speed for low quality modes to increase throughput.

In a recent printing apparatus [7], the inkjet printer switches printing speeds within a page from swath to swath depending on the ink density requirements for producing graphic and textual images. Each swath is divided into a number of partitions and depending upon the black and color ink droplets density in the partitions, firing rate and consequently carriage speed for the corresponding swath is selected. This reduces ink cartridge starvation, droplet trajectory errors and fuzzy text edges when printing high quality images while achieving higher throughput.

This paper presents the development of a motion control system that enables the implementation of an novel printer control algorithm called *Dynamic print mode control* (DPMC). DPMC optimizes the tradeoff between print quality and print speed. With DPMC, the target page is first segmented into different regions containing continuous tone image, graphics, line art and text. Appropriate print attributes are selected for each of these regions to optimize the tradeoff between print quality and speed. For example, for page regions containing images and graphics, parameters pertaining to higher quality print modes can be selected, while line art and text can be printed with parameters of higher throughput modes. One of the unique aspects of the DPMC is that the segmentation can take arbitrary shapes. In order to support DPMC, the carriage motion control system needs to be able to accept a wide variety of different motion trajectory with different print/slew speed as well as variable acceleration and deceleration profiles. In particular, due to the memory and processing constraints of the value oriented inkjet printers, the printer control algorithm will need to communicate with the carriage motion control system to dynamically update the desired motion profile based on the output of the DPMC. This will require high bandwidth carriage motion dynamics as well as integrated real-time DPMC and motion control communication. With the recent advancement of high performance digital signal processors (DSPs), it is possible to incorporate both image processing as well as real-time motion and printing control in one DSP. This paper will present the development of a high performance carriage motion controller that is designed for the next generation fixed-point DSP for DPMC.

The remaining part of the paper is organized as follows. The experimental DSP based inkjet system is briefly discussed in section 2. In section 3, the design of a TDOF digital tracking controller is discussed. Experimental and simulation results of the proposed controller are presented in section 4 followed by conclusion and summary of on-going investigations.

2. EXPERIMENTAL INKJET PRINTING SYSTEM

The experimental DSP inkjet printing system used a Lexmark Z-52 printer mechanism as the basic structure. A TIger 2.0 RIP development system is used as the development platform for DPMC and printer motion control and image processing. The Tiger system contains a TMS320C6211 DSP that is based upon the VelociTI – modified VLIW – architecture where 8 instructions can be executed in parallel at a clock speed of 150 MHz, which results in a MIPS rating of 1200. The C6211 supports pre-emptive multitasking. DSP/BIOS is the real-time operating system

The function of the cartridge transport mechanism is to carry the black and color inkjet cartridges to disperse ink droplets on the media in a direction orthogonal to the media movement. Figure 1 shows the schematic diagram of the interface between the carriage print mechanism and the Tiger development system. The carriage that holds the ink cartridges is clamped on a flexible belt, which is actuated at one end by a DC motor with a timing pulley and the other end of the belt is wrapped around a tension pulley. The DC motor is connected to an H-bridge that is driven by the 4-channel DAC0 through a current mode MOSFET PWM driver with a carrier frequency of 20 kHz. An analog PI current loop controller is implemented in hardware to achieve a 1 kHz current loop.

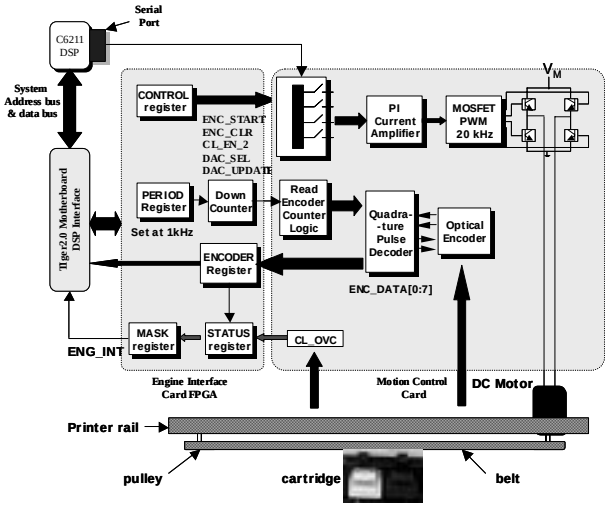

Figure 1: Schematic diagram of DSP interface to cartridge motion control mechanism.

There are five registers in the engine interface card dedicated for cartridge motion control: *encoder*, *period*, *mask*, *status* and *control* registers. Position of the cartridge on the rail is sensed through a linear incremental encoder having a resolution of 150 lpi (lines per inch). The encoder counter logic, after quadrature decoding can read the encoder counts at a programmable sampling interval and store it in the *encoder* register. Encoder sampling interval can be programmed through the *period* register. The status of various asynchronous events is shown in the *status* register and these events can be masked individually in the *mask* register. Unmasked asynchronous events send a common hardware interrupt ENG_INT to the DSP. Operation of 4-channel DAC and encoder counter is controlled through the *control* register.

3. DESIGN OF DIGITAL TRACKING CONTROLLER

3.1 System Identification of the Carriage Servo System

Figure 2 shows the block diagram of the carriage servo system with the trans-conductance amplifier, PWM and DC motor while neglecting the belt dynamics. Experimental system identification was done using the TIger2.0 system with Pseudo Random Binary Sequences (PRBS), which are sequences of rectangular pulses, modulated in pulse width, thereby approximating a discrete-time white noise signal.

Figure 3 shows a comparison of frequency response of the discrete-time spectral model computed with Blackman-Tukey method and discrete-time parametric model calculated from output error method with the fixed compensator. The phase difference between parametric model and spectral model at high frequencies results from belt dynamics coming into play, as belt is an energy storing element creating a high frequency zero.

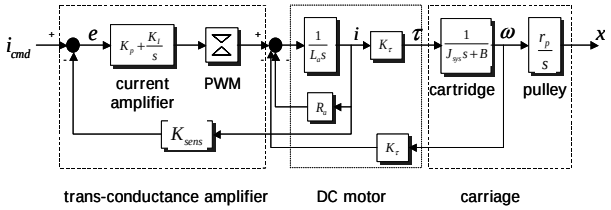

Figure 2: Schematic block diagram of carriage servo loop.

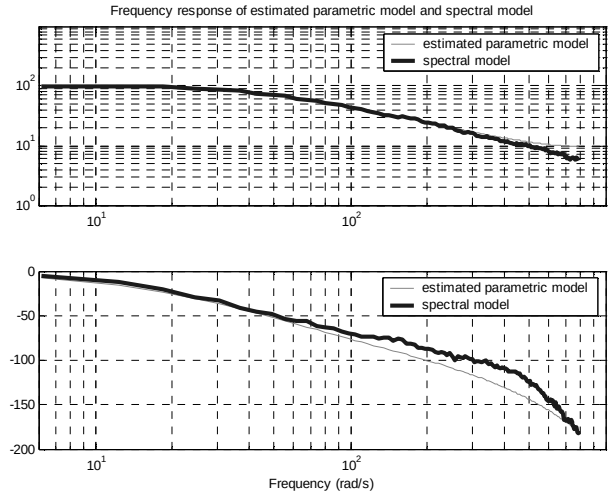

Figure 3: Comparison of frequency response of carriage motion mechanism parametric model from output error method with the spectral model from Blackman-Tukey spectral method.

The ZOH nominal models of the carriage servo system form the current command input $u(k)$ to the output variables, carriage position x(k) and velocity v(k), are given by,

$$G_{uv}^{n}(z) = \frac{v(k)}{i_{cmd}(k)} = \frac{B_{uv}^{n}(z)}{A_{uv}^{n}(z)} = \frac{4.768}{(z - 0.9536)}$$
$$G_{ux}^{n}(z) = \frac{x(k)}{i_{cmd}(k)} = \frac{B_{ux}^{n}(z)}{A_{ux}^{n}(z)} = \frac{(0.002403z + 0.002365)}{(z^2 - 1.954z + 0.9536)} \quad (1)$$

3.2 *Disturbance Observer Design for Carriage Servo System*

The carriage motion system is affected by a variety of disturbances such as stiction, sensor noise as well as unmodeled dynamics. It is desirable to be able to compensate for these disturbances, noise and unmodeled dynamics with a computationally simple disturbance observer. The disturbance observer was first proposed by Ohnishi [7] and Murakami [8] offers an attractive approach to compensate for disturbances. Compared to integral action, disturbance observer allows for more flexibility through frequency domain based tuning. Disturbance observer is typically used in the velocity loop and can improve the position loop robustness. Figure 4 shows a discrete-time version of the disturbance observer used by Kempf and Kobayashi [9].

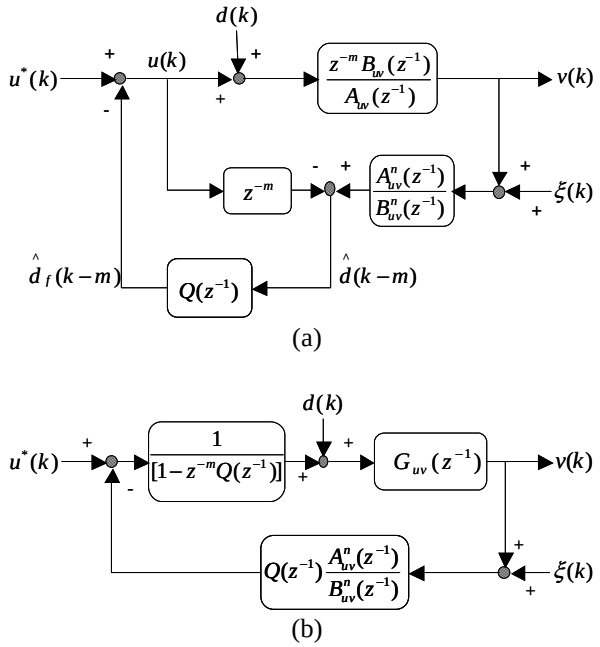

Figure 4: (a) Discrete-time disturbance observer in velocity loop and (b) Realizable discrete-time disturbance observer.

The observer regards the difference $\hat{d}(k-m)$ between the control input $u(k)$ and the output of the plant $v(k)$ (after being processed by the inverse of the nominal plant dynamics) as a result of the disturbances and plant uncertainties. This difference $\hat{d}(k-m)$ after being passed through a low pass filter $Q(z^{-1})$ gives an estimate of the disturbance. The plant output $v(k)$ is related to the various inputs by,

$$v(k)=\left[\frac{G_{uv}G_{uv}^{n}}{G_{uv}^{n}+Q(z^{-1})\left[G_{uv}-z^{-m}G_{uv}^{n}\right]}\right]\cdot u^{*}(k)-\left[\frac{G_{uv}Q(z^{-1})}{G_{uv}^{n}+Q(z^{-1})\left[G_{uv}-z^{-m}G_{uv}^{n}\right]}\right]\cdot\xi(k) \quad (2)$$
$$+\left[\frac{G_{uv}^{n}\left[1-Q(z^{-1})z^{-m}\right]G_{uv}}{G_{uv}^{n}+Q(z^{-1})\left[G_{uv}-z^{-m}G_{uv}^{n}\right]}\right]\cdot d(k)$$

Hence, neglecting sensor noise in $Q(z^{-1})$ filter's bandwidth, plant output $v(k)$ and control input $u(k)$ obey nominal plant dynamics and thereafter, open loop dynamics ensues. Since the inverse of the plant model is unrealizable, a realizable form of disturbance observer is shown in figure 4(b). $Q(z^{-1})$ is obtained by taking the bilinear transform of a continuous time Q filter:

$$Q(s)=\frac{1+\sum_{k=1}^{N-r}a_k(\tau s)^k}{1+\sum_{k=1}^{N}a_k(\tau s)^k} \quad (3)$$

where, N is the order of the $Q(s)$ filter order and r is its relative degree, which must be greater than or equal to the relative degree of the nominal plant in continuous domain. A 1st order $Q(z)$ filter with a bandwidth of 40 Hz is used in the controller design.

3.3 *Feedback Controller Design*

Since the disturbance observer can compensate for majority of the disturbance and plant uncertainty in the velocity loop, the main issue for the position loop is to achieve adequate stability robustness as well as high tracking performance. Since the disturbance observer forces the input-output plant characteristic to be close to the nominal plant model within the $Q(s)$ filter bandwidth, the need for high gain feedback controllers to reduce parameter sensitivity and improve tracking performance under uncertain friction can be avoided.

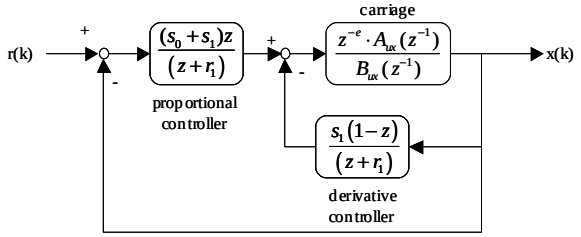

Figure 5: Fixed-point implementation of feedback controller designed by pole-placement approach.

Since the open loop system has inherent integrator dynamics with a long time constant, to stabilize and speed up the dynamic response of the system, a PD controller is sufficient. The PD controller is designed in discrete-time domain using a pole placement approach. A closed loop bandwidth of 5 Hz and a damping ratio of 0.98 were selected to give the best performance for fixed-point implementation. The dominant second order closed loop poles are located at,

$$p_1=-e^{-\xi\omega_n T}+je^{-\sqrt{1-\xi^2}\omega_n T} \text{ and } p_2=-e^{-\xi\omega_n T}-je^{-\sqrt{1-\xi^2}\omega_n T} \quad (4)$$

where, $\omega_n=2\cdot\pi\cdot 5$ rad/sec, T=0.001 sec and ξ=0.98.

The closed loop characteristic polynomial for the feedback controller is,

$$
\begin{aligned}
A_{CL} &= A_{ux}(z)\cdot R(z) + B_{ux}(z)\cdot S(z) \\
&= \left[A_{ux}(z)\cdot \bar{R}(z) + B^{-}_{ux}(z)\cdot S(z) \right]\cdot B^{+}_{ux}(z) \qquad (5) \\
&= A_m(z)\cdot A_o(z)\cdot B^{+}_{ux}(z)
\end{aligned}
$$

where, $B^{+}(z)$ and $B^{-}(z)$ contain the cancelable and uncancelable zeros of the plant model, respectively. $A_m(z)$ is the desired closed loop polynomial containing poles p_1 and p_2. For a unique solution to Eq. (5), $A_{CL}(z)$ is of the order 3. Let $A_o(z) = (z+a_1)$. The feedback controller is then of the form,

$$
\begin{aligned}
C_{fd}(z) &= \frac{(s_0 z + s_1)}{(z + r_1)} = \frac{(s_0 + s_1)z - s_1(z-1)}{(z + r_1)} \\
&= \frac{(s_0 + s_1)z}{(z + r_1)} - \frac{s_1(z-1)}{(z + r_1)} \qquad (6) \\
&= \frac{(0.7197z - 0.6751)}{(z - 0.7653)}
\end{aligned}
$$

The feedback controller has a proportional gain of (s_0+s_1) and a derivative gain of s_1 with a low pass filter pole at r_1.

To reduce the effect of quantization during fixed-point computation and increase the robustness to disturbance, the derivative part of the controller operates on the position output and the proportional part operates on the error between the reference command and the actual position as shown in Figure 5. The first order closed loop pole at $z = -a_1$ is adjusted to obtain the desired disturbance and quantization noise rejection characteristics. Figure 6 shows the frequency response of the closed loop transfer function (i.e. complementary sensitivity function), the open loop transfer function, and the system sensitivity function. The disturbance observer reduces the need for a high gain feedback controller to overcome friction and reduces the system's sensitivity to parameter variation.

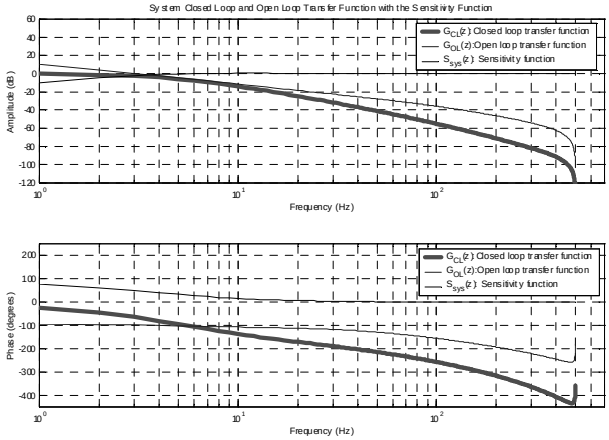

Figure 6: Frequency response of the system open loop transfer function, closed loop transfer function (or complementary sensitivity function) and sensitivity function.

3.4 Feedforward Controller Design

In the current implementation of the DPMC, a portion of the desired carriage trajectory can be computed before the cartridge starts printing, a feedforward controller can be used to take advantage of this preview information to reduce dynamic lag in the closed loop system and improve tracking performance. To meet the print quality requirements, both the position and velocity tracking errors need to be minimized.

The tracking problem can be broken down into four categories (Tomizuka [10]) depending upon the amount of knowledge available about the desired trajectory. Carriage tracking control problem belongs to the 1st or 2nd category, where a potion of the desired position and velocity trajectory can be calculated in advance or for some time interval.

Zero Phase Error Tracking (ZPET) controller while inverting the closed-loop dynamics also takes into account the unstable or uncancelable zeros of the closed loop system. If the closed loop system is given by,

$$
G_{CL}(z^{-1}) = \frac{z^{-d}\cdot B_{CL}(z^{-1})}{A_{CL}(z^{-1})} = \frac{z^{-d}\cdot B^{+}_{CL}(z^{-1})\cdot B^{-}_{CL}(z^{-1})}{A_{CL}(z^{-1})} \qquad (7)
$$

where, $B^{+}_{CL}(z^{-1})$ and $B^{-}_{CL}(z^{-1})$ are the cancelable and uncancelable/unstable zeros of the closed loop system, respectively. d is the number sampling period delay. The corresponding ZPET controller transfer function is given by,

$$
\begin{aligned}
G_{ZPET}(z^{-1}) &= \frac{z^{d}\cdot A_{CL}(z^{-1})\cdot B^{-}_{CL}(z)}{B^{+}_{CL}(z^{-1})\cdot \left[B^{-}_{CL}(1) \right]^2} \\
&= \frac{z^{d+s}\cdot A_{CL}(z^{-1})\cdot B^{*-}_{CL}(z^{-1})}{B^{+}_{CL}(z^{-1})\cdot \left[B^{-}_{CL}(1) \right]^2},
\end{aligned} \qquad (8)
$$

where, $z^{-s}\cdot B^{-}_{CL}(z) = B^{*-}_{CL}(z^{-1})$

With the feedback controller in place, the closed loop transfer function of the carriage motion control system is given by,

$$
G_{CL}(z^{-1}) = \frac{0.0001072\cdot z^{-2}\cdot \left(1 + 0.9843z^{-1}\right)}{\left(1 - 2.717z^{-1} + 2.449z^{-2} - 0.7313z^{-3}\right)} \qquad (9)
$$

Without inverting the marginally stable zero from the carriage model, the ZPET controller is given by,

$$
G_{ZPET}(z^{-1}) = \frac{z^3\cdot \left(1 - 2.717z^{-1} + 2.449z^{-2} - 0.7313z^{-3}\right)\cdot \left(1 + 0.9843z^{-1}\right)}{0.0001072\cdot \left(1 + 0.9843\right)^2} \qquad (10)
$$

Figure 7 shows the frequency response of the ZPET controller. To prevent the amplification of high frequency noise, a zero phase low pass (ZPLP) filter is combined with the ZPET controller. A unity gain ZPLP filter is given by,

$$
\begin{aligned}
G_{ZPLP}(z^{-1}) &= \frac{\left(\alpha_l z^{l} + \mathrm{L} + \alpha_1 z^{1} + \alpha_0 + \alpha_1 z^{-1} + \mathrm{L} + \alpha_l z^{-l}\right)}{\left(\alpha_0 + 2\alpha_1 + \mathrm{L} + 2\alpha_{l-1} + 2\alpha_l\right)} \qquad (11) \\
&= \frac{z^{l}\cdot \left(\alpha_l + \mathrm{L} + \alpha_1 z^{-l+1} + \alpha_0 z^{-l} + \alpha_1 z^{-l-1} + \mathrm{L} + \alpha_l z^{-2l}\right)}{\left(\alpha_0 + 2\alpha_1 + \mathrm{L} + 2\alpha_{l-1} + 2\alpha_l\right)}
\end{aligned}
$$

The addition of the ZPLP filter requires extra preview steps (ZPLP filter's relative degree *l*) in addition to the ZPETC's preview steps (*d*+*s*). Choosing a small *l* affects the filter performance during fixed-point computation due to coefficient quantization and scaling. However, it can be trade-off by the savings in computation time. For the carriage servo system, the ZPLP filter cut-off frequency is chosen to be 50 Hz and the length of the ZPLP filter is 3, or of 2nd order. Figure 7 shows the frequency response of the ZPET controller and the ZPLP filter. The overall carriage motion control system block diagram is shown in Figure 8.

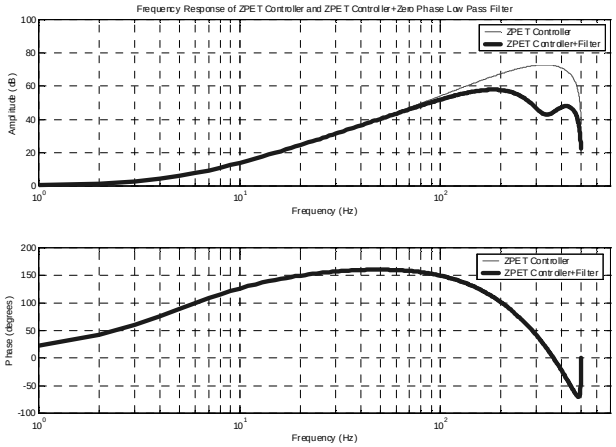

Figure 7: Frequency response of ZPET controller and ZPET controller + Zero phase low-pass filter.

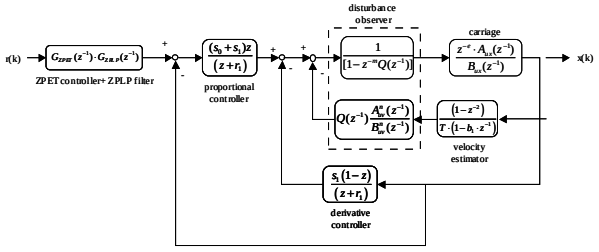

Figure 8: Carriage motion control structure.

4. Experimental Results

The swath parameters used for the experiment are given in Table 3. The carriage speeds for monochrome printing (Table 2) are used for each print zone. The controller is implemented on the C6211 using 16 bit fixed-point arithmetic. Significant time has been invested to reduce the computation time as well as identifying the proper scaling factor to preserve the computation accuracy without overflowing the data registers.

Figure 9 shows the phase plot (velocity vs. position) of the carriage motion during a typical swath that contains the three print zones specified in Table 3. The phase plot of carriage velocity vs. carriage position reveals the performance requirements as the carriage is required to reach a desired printing velocity at a specific print zone start position. As can be seen from Figure 9, the experimental data matches well with the desired command as well as the simulation results.

Table 3: Swath parameters used for testing cartridge motion controller.

Print Zone	Start position (inch)	Stop position (inch)	Velocity (ips)
1	0.75	1.75	20
2	2.50	4.50	20
3	5.00	7.00	30

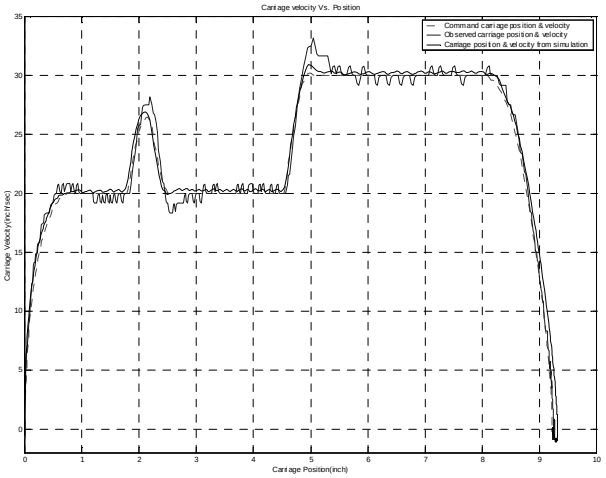

Figure 9: Experimental and simulated carriage velocity vs. position for a swath that contains three print zones.

Figure 10 shows the experimental time history of the carriage acceleration and motor current command. During constant velocity, coulomb friction is compensated by a motor current of approximately 0.2 Amp. Figure 11 shows the time history of the corresponding carriage position and velocity error. The carriage position error is about 0.06 inch at 20 ips and 0.08 inch for 30 ips. This does not affect uni-directional printing as the position error is same for all swaths, but bi-directional printing gives rise to text and image artifacts if proper position offsets are not provided. The carriage velocity error during the constant speed portion (print zone) of the motion is less than 1 inch/sec or 1 count/sample, which is within the sensor (encoder) resolution level and is well within the performance requirement. Also, the carriage accelerates and decelerates between two successive print zones having the same printing velocity, i.e. the carriage is performing horizontal white space skipping between two print zones.

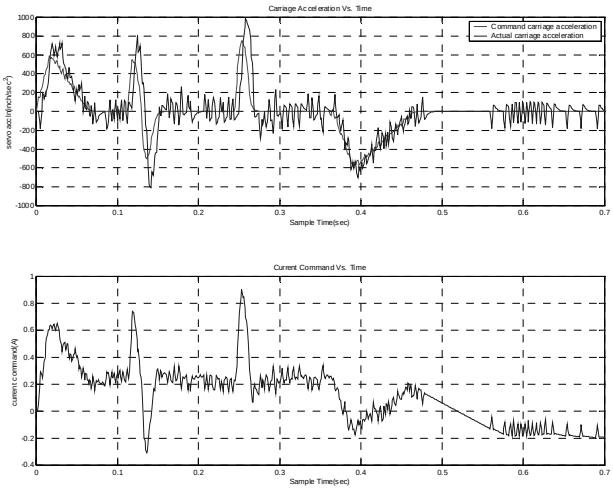

Figure 10: Experimental and command carriage acceleration and motor current (control effort)

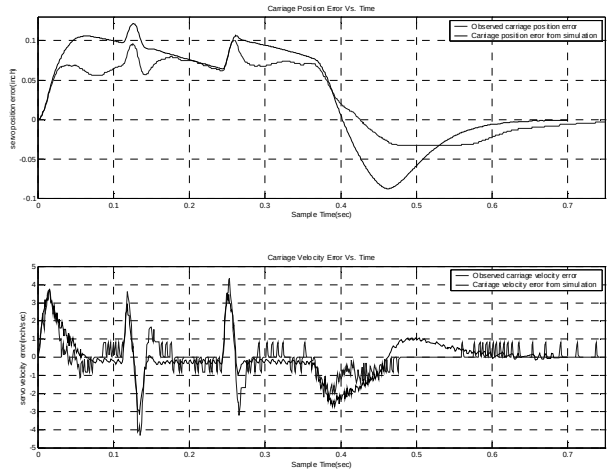

Figure 11: Experimental and simulated carriage position and velocity error for a typical swath.

The introduction of a low order ZPLP filter (l=2) and coefficient quantization due to fixed-point implementation introduced a slight mismatch in steady-state gain between the ZPET+ZPLP filtered command carriage position and desired command position trajectory. To compensate for the steady-state position error while minimize the computation overhead, the feedforward controller is switched off once the carriage has traversed the command trajectory, i.e. the system is in regulation mode. It took an addition 0.1 sec. for the carriage to converge to the desired final location. The final position accuracy is not important during printing, as long as it provide adequate acceleration distance for the subsequent swath.

5. CONCLUSION

A carriage motion controller was designed based on a ZPET+DOB based TDOF design approach. To reduce the computation time, the controller is implemented using fixed-point arithmetic and re-structured scaled to minimize the effect of quantization. Experimental results show the operational capability of carriage motion controller to perform horizontal white space skipping and dynamic change of carriage motion attributes as required by DPMC. The system has been successfully implemented for uni-directional and bi-directional monochrome printing. Work is under way to extend the system to color images.

6. REFERENCES

1. J.L.K. Chan and A.B. Tan, "Variable-Duration Printer Carriage Motor Acceleration Method and Apparatus", U.S. Patent: 5,627,947, *Hewlett-Packard Co*., Palo Alto, CA USA, May 6, 1997.
2. J.C. Santon and J.H. Bauman, "Method and Apparatus for achieving Increased Printer Throughput", U.S. Patent: 5,669,721, *Hewlett-Packard Co*., Palo Alto, CA USA, Sept. 23, 1997.
3. K. Kawazoe, "Recording Apparatus, Method and Information Processing System", U.S. Patent: 5,871,291, *Canon Inc*., Tokyo Japan, Feb. 16, 1999.
4. K. Yokoi and M. Wataya, "Printing Apparatus and Printing Method thereof", U.S. Patent: 5,873,663, *Canon Inc*., Tokyo Japan, Feb. 23, 1999.
5. S.H. Lee, "Technique for Controlling the Position of a Driving Motor and a Printhead", U.S. Patent: 6,000,869, *Samsung Electronics Co. LTD*., Suwon S. Korea, Dec. 14, 1999.
6. J.P. Bolash and E.H. James III, "Asymmetrical Acceleration Ramp Area Method for Print Cartridge Carrier of Inkjet Printer", U.S. Patent: 5,997,130, *Lexmark Inter. Inc.*, Lexington, Kentucky USA, Dec. 7, 1999.
7. Ohnishi K., "A New Servo Method in Mechatronics", *Transactions of Japanese Society of Electrical Engineering*, Vol. 107-D, pp. 83-86, 1987.
8. T. Murakami and K. Ohnishi, "Advanced Motion Control in Mechatronics – A Tutorial", *Proceedings of IEEE Inter. Workshop on Intelligent Control*, Vol. 1, pp. SL9-SL17, August 1990.
9. C.J. Kempf and S. Kobayashi, "Disturbance Observer and Feedforward Design for a High Speed Direct Drive Positioning Table", *IEEE Transactions on Control Systems Technology*, Vol. 7, No. 5, pp. 513-526, September 1999.
10. M. Tomizuka, "Feedforward Digital Tracking Controllers for Motion Control Applications", *Journal of Advanced Robotics*, Vol. 7, No. 6, pp. 575-586, 1993
11. M. Kamasak, A.V. Deshpande, K.L. Thoon, C. Bouman, G.T.-C. Chiu, and J. Allebach, "Dynamic Print Mode Control for Inkjet Printing," in the *Proceedings of the IS&T NIP17: International Conference on Digital Printing Technologies*, pp. 78-82, Ft. Lauderdale, Florida, September 30-October 5, 2001.